



Regular Article

Prioritization of Susceptibility Zones for Multi-Hazard Risk in Jammu Division of the North-West Himalayas, India for Disaster Risk Reduction

Lucky Sharma^{1*} and Narendra Kumar Rana¹

Received: 24/07/2023 / Accepted: 08/06/2024 / Published online: 06/08/2024

Abstract Environmental hazards have always been a source of serious concern as they are becoming more severe and wider in scope, enhancing the risk of additional losses to the environment and public health. The comprehensive risk assessment has emerged as a core component of disaster mitigation strategy. After the international convention on sustainable development in 1992, the multi-hazard approach is widely used as part of Disaster Risk Reduction (DRR) strategy. Lying in the vicinity of the North-West Himalayan region, Jammu Division is prone to multiple hazards which have led to numerous casualties. In this study, landslides, floods, earthquakes, droughts, forest fires and soil erosion are considered for prioritizing risk from multi-hazard. Analytical Hierarchy Process have been adopted for data processing for the standardisation and normalisation of the weights. The area prone to multiple hazards is delineated after overlaying all the individual assessment of hazard events using weights computed by an objective approach. The multi-hazard susceptibility map is categorised into five zones: very low, low, moderate, high and very high. The findings revealed that 43.43 % of area lying in south eastern, central and eastern part is suffering from multiple hazards are prioritized for preventing communities to suffer from the multiple hazards. This area lies in central part of the study area in proximity to faults and weak lithology. The identified area under multi-hazard should be well studied for potential cascading of hazards. The targeted interventions and proactive measures should be adopted for enhancing the resilience and disaster risk reduction. The prioritized zones will be extremely valuable for risk profiling, vulnerability assessment and formulation or revision of DRR strategy action plans.

Keywords: Multi-hazards, Susceptibility assessment, Analytical Hierarchy Process, Disaster Risk Reduction, Risk profiling

¹ Department of Geography, Banaras Hindu University, India
* Corresponding author email: imlucky1512@gmail.com

1. INTRODUCTION

Environmental hazards pose a serious threat to public health and assets (Javidan et al., 2021; Morales & de Vries, 2021). The damage from hazards has been increasing considerably (Pouyan et al., 2021) as the recent United Nation Disaster Risk Report (UNDRR), 2022 supported that continual addition has been reported in disaster events per year, moreover, it is projected that the number of events could reach 560 by 2030 as opposed to 400 in 2015 (UNDRR, 2022). Since the risk of single hazard has been on rise, the impact is never single fold rather it is multi-fold. The impact of any hazard is increased and worsened by the interaction of another hazard as the occurrence of one hazard is more often followed by another (Liu et al., 2016; Eshrati et al., 2015). Previous studies indicate that researchers have predominantly focused on studying single hazards as evidenced by the works of Javidan et al., 2021; Pouyan et al., 2021; Kappes et al., 2012. For instance, hazards like landslides (Althuwaynee et al., 2014; Pellicani et al., 2017; Dasanayaka & Matsuda, 2022), floods (Kazakis et al., 2015; Kabenge et al., 2017; Aydin & Birincioglu, 2022), earthquakes (Theilen-Willige 2010; Dhar et al., 2017), drought (Lehner et al., 2006; Palachaudhari & Biswas, 2016), soil erosion (Aslam et al., 2021), tropical cyclones (Hoque et al., 2018), and forest fires (Adab et al., 2013; Gheshlaghi et al., 2020) are among the few examples that have been studied as individual hazards.

In recent times, there has been a discernible shift in attention from individual hazard evaluation to multi-hazard studies, driven by the recognition that hazards occur differently across locations and can interact with one another (Tilloy et al., 2019). The term multi-hazard got recognition in Agenda 21, when the multi-hazard approach was adopted for Disaster risk reduction followed by the Johannesburg plan and Hyogo framework of action 2005-2015 (Eshrati et al., 2015; Kappes et al., 2012). The concept of multi-hazards can be well understood by these definitions- “totality of all the relevant hazards at place” (Kappes et al., 2011), “all-hazards-at-place” (Hewit & Burton, 1971) or “multiple hazards that country faces” (UNDRR, 2009). In the words of Kappes et al., 2012, all multi-hazard studies generally involve more than one hazard approach. Being location-specific (Morales & de Vries, 2021), a hazard may occur only at certain places or multiple hazards can exist in any geophysical environment (Angeli et al., 2022; Kappes et al., 2012).

Geographical Information Systems (GIS) and remote sensing have been effective and useful in the field of hazard vulnerability and risk studies (Berry, 2009; van Westen, 2011). By employing visual aids and thorough examination, hazard mapping empowers stakeholders to recognize potential dangers, evaluate susceptibilities, and devise proactive strategies to reduce negative consequences (Pimentel et al., 2020). As a proactive response and mitigation strategy, multi-hazard mapping has proven to be the most beneficial and effective (van Western & Grieving, 2017). Multi-hazard mapping has become popular and sophisticated as there is no single approach developed to assess multi-hazards risk (Pourghasemi & Kerle, 2016, Aksha et al., 2020). Several methodologies (Morales & de Vries, 2021) have been

developed such as Multi-criteria decision Methods-Analytical hierarchy process (AHP)/Fuzzy AHP (Morales & de Vries, 2021; Aksha et al., 2021;), Analytical Network Process, Machine learning Methods- Support Vector Machine (SVM), General Linear Model (GLM), Boosted Regression Tree (BRT) (Rahmati et al., 2019; Pouyan et al., 2021), Convolution Neural Network (CNN) (Ullah et al., 2022), Random Forest (RF) (Pouyan et al., 2021), MaxEnt (Javidan et al., 2021) have been deployed to map the multi-hazard. In this present study, the Multi-criteria AHP method which is developed by Saaty in 1980 (Saaty, 2008) is employed in a GIS environment to prepare maps. The AHP method has gained widespread popularity, especially in hazard assessment (Morales & de Vries, 2021) and it is frequently applied in integration with GIS and remote sensing (Psomas et al., 2018). Its significance lies in the fact that it entails expert participation to remove the pure subjectivity involved in decision-making and weighing criteria (Zizovic et al., 2020).

2. STATEMENT OF THE PROBLEM

The Himalayan belt and adjoining portion of the alluvial plain are notoriously unstable and vulnerable to multiple hazards (Patel et al., 2020). Despite the area's proneness to disaster due to topography and relief, stress related to hazards is surging continuously because of the increasing populace and paced construction work (Patel et al., 2020; Yousuf et al., 2017). Earthquakes, floods, landslides, avalanches, flash floods, cloud bursts etc. happen frequently according to earlier studies (Chandra et al., 2018; Kumar and Acharya, 2016; Thayyen et al., 2013). Ali et al. (2022) while preparing profile of hazard of the Kashmir Himalaya (part of NW Himalaya) summarize 1693 earthquakes, 39 floods, 65 landslides, and 57 snow avalanches events signify the severity and adversity of natural hazards in the region. Another factor that has contributed to the disasterisation of hazards is political unrest (Shah et al., 2018). Hence, it becomes imperative for us to assess multi-hazard as the need of the hour.

3. STUDY AREA

The study area encompasses the North-Western Himalayan and adjoining Punjab plains. The present study attempts to cover only the Jammu division of Union Territory of Jammu and Kashmir (UT J&K) (Figure 1). Jammu division is comprising ten districts: Jammu, Punch, Reasi, Rajouri, Udhampur, Samba, Kathua, Doda, Ramban, and Kishtwar. It stretches between 32°17' to 34°12' N latitude and 73°58' to 76°47' E longitude (Sharma, 2019). It is surrounded by Kashmir valley in the north, UT of Ladakh in the west, and Punjab and Himachal Pradesh in the south. Jammu province varies in altitude from 300 metres above mean sea level (AMSL) to above 6000 AMSL. Topographically, the Jammu province is divided into three divisions: Alluvial plains (south), Outer Himalayas, and Middle Himalayas (Sharma, 2019). The great diversity is found in the temperature and precipitation distribution

of the Jammu division. In summer, the temperature goes as high as 45°C in the southern alluvial plains whereas it doesn't exceed more than 32°C in the mountainous part of the region. However, as low as -10°C is observed in Middle Himalayas during winters. Annual rainfall varies between 60cm to 150cm (IMD, 2014). The region is predisposed to multiple hazards (Patel et al., 2020) and has faced massive hazards like the 2005 earthquake, and 2014 flood, landslide and avalanches are seasonal phenomena (SDMP, 2017) (Table 1). Hassan (2014) also mentioned the occurrence of occasional droughts in the region.

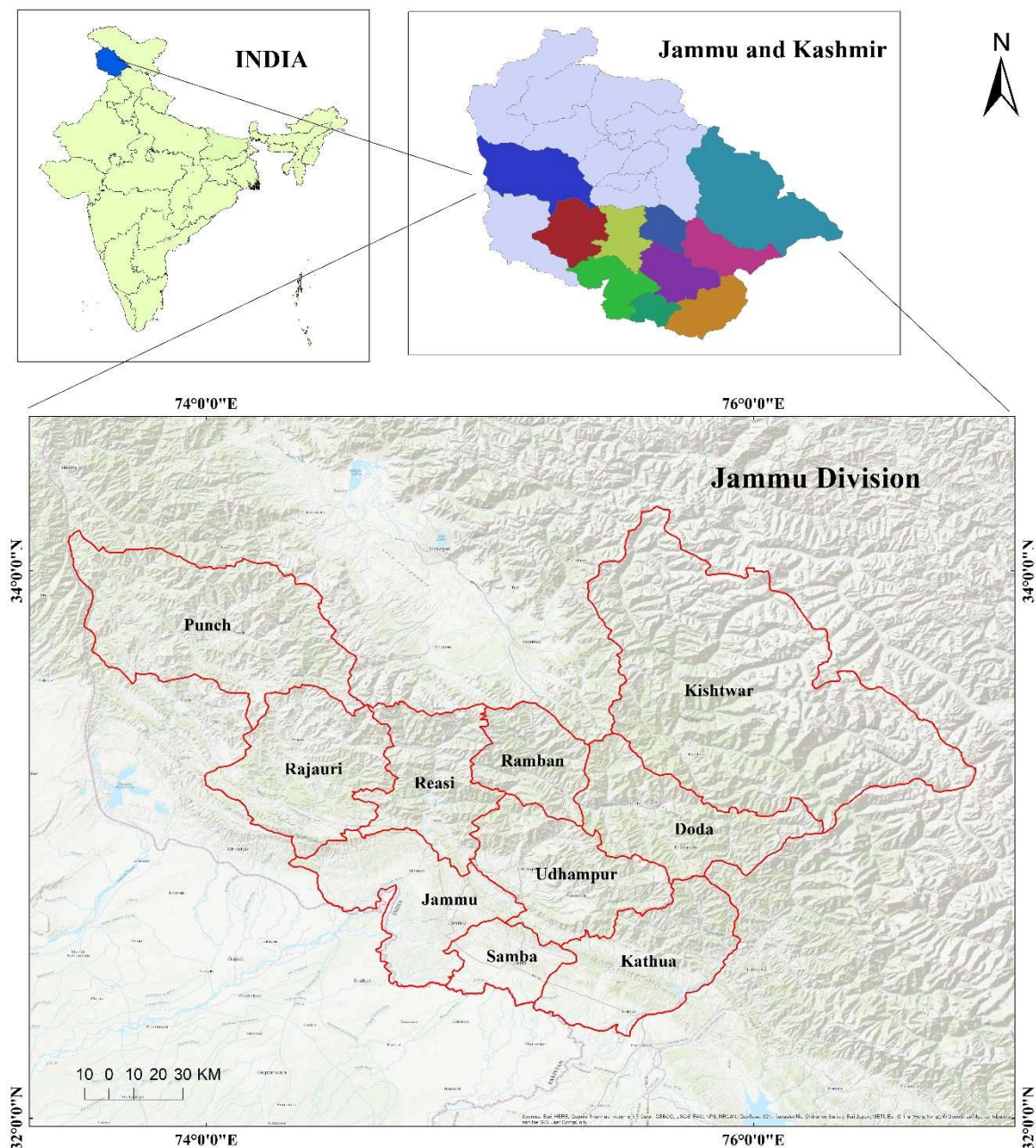


Figure 1. Location map of the study area

Table 1. Major disaster events and losses in the study area

S.no.	Major events	Causalities held
1.	Jammu and Kashmir Earthquake, 2005	7.6 richter scale, 23782 houses were damaged and 953 death
2.	Doda Cloud Burst and flash floods, 2011	17 ststructure washed away, many lives drown into flash floods
3.	Jammu and Kashmir Floods, 2014	over 300 lives, 2 million affected and 2.53 lakh house damaged, a vilage sadal alone experienced 40 deaths
4.	Thatri, Doda, Cloud burst and flash floods, 2017	8 people killed, 11 injured, resultant flashflood inundated Doda-Banihal-Kishtwar highway

Source: State Disaster Development Plan, 2017; Patel et al., 2020

4. RESEARCH OBJECTIVE

The present work aimed to create a multi-hazards map by aggregating the six hazards-earthquake, floods, landslide, forest fires, soil erosion and droughts. The novelty of the present study is that it has involved six hazards at once and their weight are computed using objective approach considering frequency and total damages caused by hazard.

5. MATERIAL AND METHODS

5.1 Database and Source

According to previous existing literature, usually, fifteen to twenty-one factors (Khatakho et al., 2021; Ullah et al., 2022; Sanam et al., 2022) have been considered to map multi-hazards whereas, in the present study, twenty factors have been selected for hazard assessment. For each hazard, selected factors are discussed in Table 2 and Figure 2a-2t. The format and sources of data are discussed in Table 3 and their brief description is given below one by one.

Table 2. Selected causative factors for each hazard for preparing the multi-hazard map

Layers	Earthquakes	Flood	Landslide	Forest Fire	Drought	Soil Erosion
Distance From Fault	×		×			
Flow Accumulation	×	×				
Slope	×	×	×	×	×	×
Elevation	×	×	×	×		×
Drainage Density		×				×
Land Use		×	×	×	×	×
Geology	×	×	×			×

Annual Precipitation	×	×	×	×	×
Distance To Stream	×				
TWI	×				
Curvature	×				×
Aspect		×	×		
Soil	×	×		×	
NDVI		×		×	×
Temperature			×	×	
Wind Speed			×		
Evapotranspiration				×	
Maximum				×	
Temperature					
Lineament Density		×			×
Relative Humidity				×	

Note: × represent the selected factor

Table 3. Description of causative factors showing their sources and format

Factors	Source	Format	Resolution
Distance From Fault	Bhukosh, Geological Survey Of India	Polylines	-
Flow Accumulation	Extracted From CARTODEM*	Raster	30m
Slope	Extracted From CARTODEM	Raster	30m
Elevation	CARTODEM Downloaded From BHUVAN^	Raster	30m
Drainage Density	Extracted From CARTODEM	Raster	30m
Land Use	Sentinel-2 Imagery, 2021	Raster	10*10m resolution
Geology	USGS Geology Atlas	Polygon	-
Annual rainfall	Climate Research Unit (CRU) Database	NetCDF	(°5x °5 grid)
Distance To Stream	Extracted From CARTODEM*	Raster	30m
TWI	Extracted From CARTODEM	Raster	30m
Curvature	Extracted From CARTODEM	Raster	30m
Aspect	Extracted From CARTODEM	Raster	30m
Soil	Food And Agricultural Organisation, FAO	Polygon	-
NDVI	Oceansat 2, Download From BHUVAN	Raster	30m
Temperature	POWER NASA* Database	Point And Attribute	-
Wind Speed	Global Wind Atlas	Raster	30m
Evapotranspiration	MODIS*, USGS Earth Explorer	Raster	30m
Maximum Temperature	POWER NASA Database	Point And Attribute	-
Lineament Density	Bhukosh, Geological Survey Of India	Polylines	-
Relative Humidity	POWER NASA Database	Point And Attribute	-

5.2 Description of Causative Factors

Geology and Distance to Faults: The role of geology is immense in governing the earthquake, landslide, flood and soil erosion hazards (Pourghasemi & Kerle, 2016; Nsangou et al., 2021). The geology of the study area is downloaded from USGS World Geologic maps (Figure 2s) and fault line in the form of Polylines is downloaded from Bhukosh, the official web portal of the Geological Survey of India. Distance to Fault has been prepared from the

multiple ring buffer tool of Aeronautical Reconnaissance Coverage Geographic Information System (ArcGIS) Software version 10.5 with a distance of 10 km intervals (Figure 2d).

Lineament Density: Lineament density is extracted from Lineament which is downloaded from the Bhukosh, web portal of the Geological Survey of India and it is prepared in ArcGIS using the Euclidean distance tool (Figure 2e). It controlled curvilinear features according to Sonker et al., 2021 and hence represent fracture and fault zones. In the study area, the Main central thrust and the Himalayan central thrust are both found that make the area susceptible to landslides, floods, and soil erosion.

Drainage Density: It substantially impacts floods (Paul et al., 2019) and there exists the direct relationship between flood and drainage density (Ullah & Zhang, 2020). Drainage density is determined from the DEM and mapped using the line density technique of the spatial analysis tool in ArcGIS (Figure 2g).

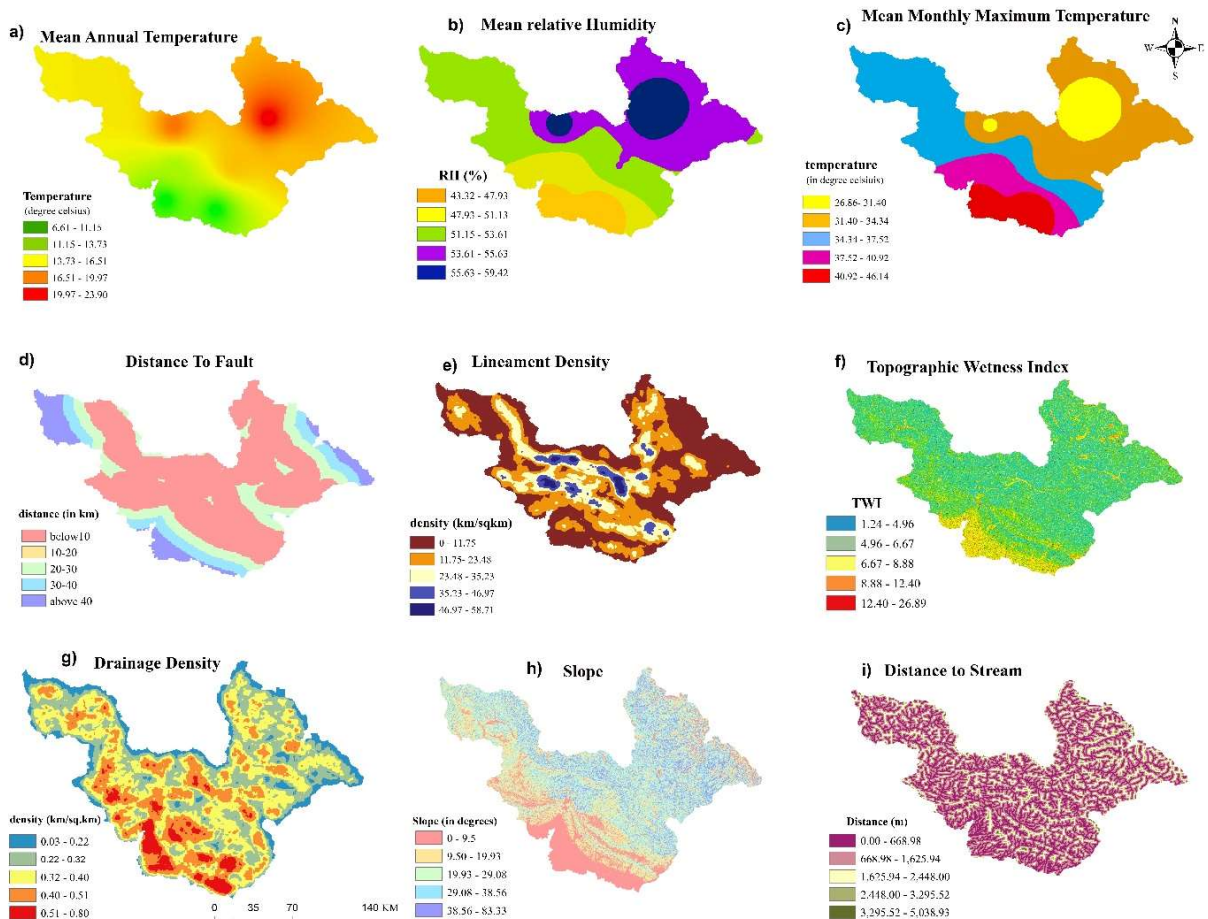


Figure 2a-2i. Mean annual temperature, Mean relative humidity, Mean monthly maximum temperature, Distance to fault, Lineament density, TWI, Drainage density, Slope and Distance to stream

Slope: It is of paramount importance in influencing almost all the hazards whose thematic layer was prepared from DEM using the slope of 3D analysis tool in ArcGIS Software version 10.5 (Figure 2h). Steeper slopes are known to be more susceptible to erosion,

landslide and earthquake whereas floods tend to occur in those areas where gentle slopes are found (Rincoin et al., 2017; Saini et al., 2015; Dou et al., 2020; Kaur et al., 2019).

Mean Annual Temperature: The study used the Prediction of Worldwide Energy Resource (POWER) project of the National Aeronautics and Space Administration (NASA) for extracting annual temperature data which is collected in the form of attributes of a particular location. The IDW interpolation technique is used to obtain the final map (Figure 2a). The temperature plays a decisive role in determining the vulnerability of forest fire and drought susceptibility (Lamat et al., 2021; Palachudhuri & Biswas, 2016).

Mean Relative Humidity: Relative humidity is one of the important climatic factors that play a crucial role in determining drought susceptibility (Palachudhuri & Biswas, 2016). It is downloaded in attribute form from the POWER project database of NASA for forty years and its map is prepared using the IDW technique in ArcGIS (Figure 2b).

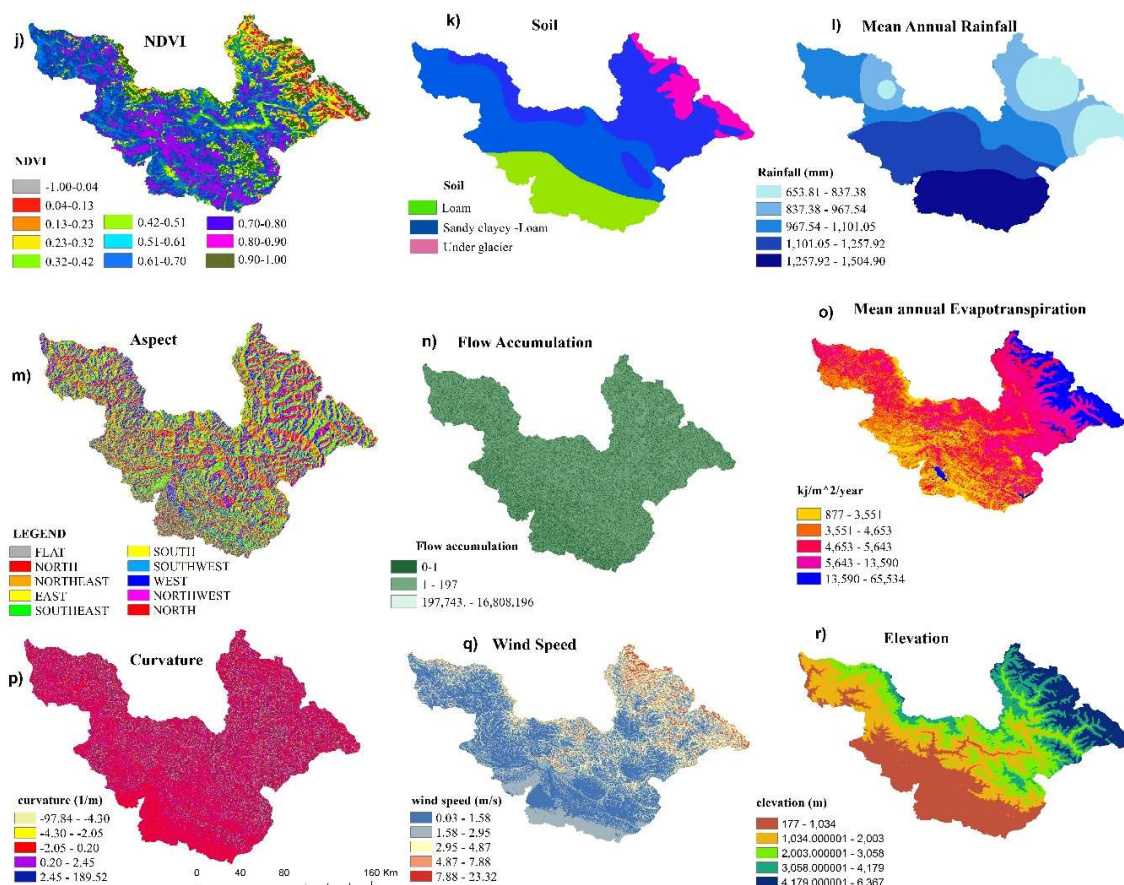


Figure 2j-2r. NDVI, Soil, Mean annual rainfall, Aspect, Flow accumulation, Mean annual evapotranspiration, Curvature, Wind speed, and Elevation

Mean maximum Temperature: Another significant factor contributing to drought susceptibility is mean maximum temperature (Palachudhuri & Biswas, 2016) which is also extracted from the POWER project database of NASA in attribute form. IDW technique is applied to create the layer (Figure 2c).

Topographic Wetness Index (TWI): The TWI is a measure of the influence of local topography on surface hydrology which reflects the possibility of water infiltration capacity (Arulbalaji et al., 2019, Khosravi et al., 2016). In the current study, TWI is determined from DEM and is mapped (Figure 2f) using the following formula as:

$$TWI = \ln(\alpha / \tan\beta)$$

whereas α represents the accumulation of flow and $\tan\beta$ represents associated slope.

Normalised Difference Vegetation Index (NDVI): The NDVI is utilised to examine the vegetative cover and its influence on slope stability, runoff and infiltration (Khatakho et al., 2021; Fang et al., 2021). It is inversely proportional to landslide susceptibility (Khatakho et al., 2021). NDVI developed by utilising Oceansat-2 downloaded from Bhuvan, web portal of NRSC, Government of India (Figure 2j). Its value ranges between -1 to 1.

Soils: The texture of the soil is an important factor that influences infiltration and runoff leading to many hazards. The data regarding the soil is downloaded from Food and Agricultural Organisation (FAO) in polygon forms whose map is prepared in ArcGIS (Figure 2k).

Distance to Stream: Distance to stream is another crucial factor in governing floods (Khosravi et al., 2016). The proximity of an area to streams makes them vulnerable during the season of heavy rainfall (Das, 2019). It is extracted from DEM and mapped using the Euclidean distance tool in ArcGIS (Figure 2i).

Annual Rainfall: It is one of the triggering factors of landslides, floods soil erosion and its deficiency leads to drought (Bennet et al., 2018; Long et al., 2018). The data on precipitation is collected for 40 years on average from 1981-2021 in gridded form from the Climate Research Unit gridded Time Series (CRUTS) database downloaded from <https://crudata.uea.ac.uk/cru/data/hrg/> (data viability is shown in Harris et al., 2020). After converting the gridded data into point form, the Rainfall map is prepared using Inverse Distance Weighted (IDW) interpolation technique in ArcGIS (Figure 2l).

Aspect: Aspect is one of the topographic factors that is derived from DEM using the aspect of the 3D analysis tool in ArcGIS (Figure 2m). Khatakho et al., 2021 mentioned aspect as an aggravating factor for landslides which influence the hydrological process, meteorological, and morphological structure of an area (Ullah & Zhang, 2021, Yalcin, 2008).

Curvature: It aids in concentrating the water on the concave side (Khatakho et al., 2021). In this study, the curvature (Figure 2p) is derived from the DEM in ArcGIS which shows the topographic shape of the area (Das, 2019).

Flow Accumulation: It is considered one of the important causative factors for earthquakes and floods (Aksha et al., 2020). It is extracted and prepared from DEM using the hydrology tool in ArcGIS (Figure 2n).

Wind Speed: It is another factor contributing to the intensity of forest fire mainly in the present study (Adab et al., 2013; Schoennagel, 2004) whose data is downloaded from Global Wind Atlas in Raster form (Figure 2q). The wind speed at the 10m exposure map is extracted from the downloaded raster.

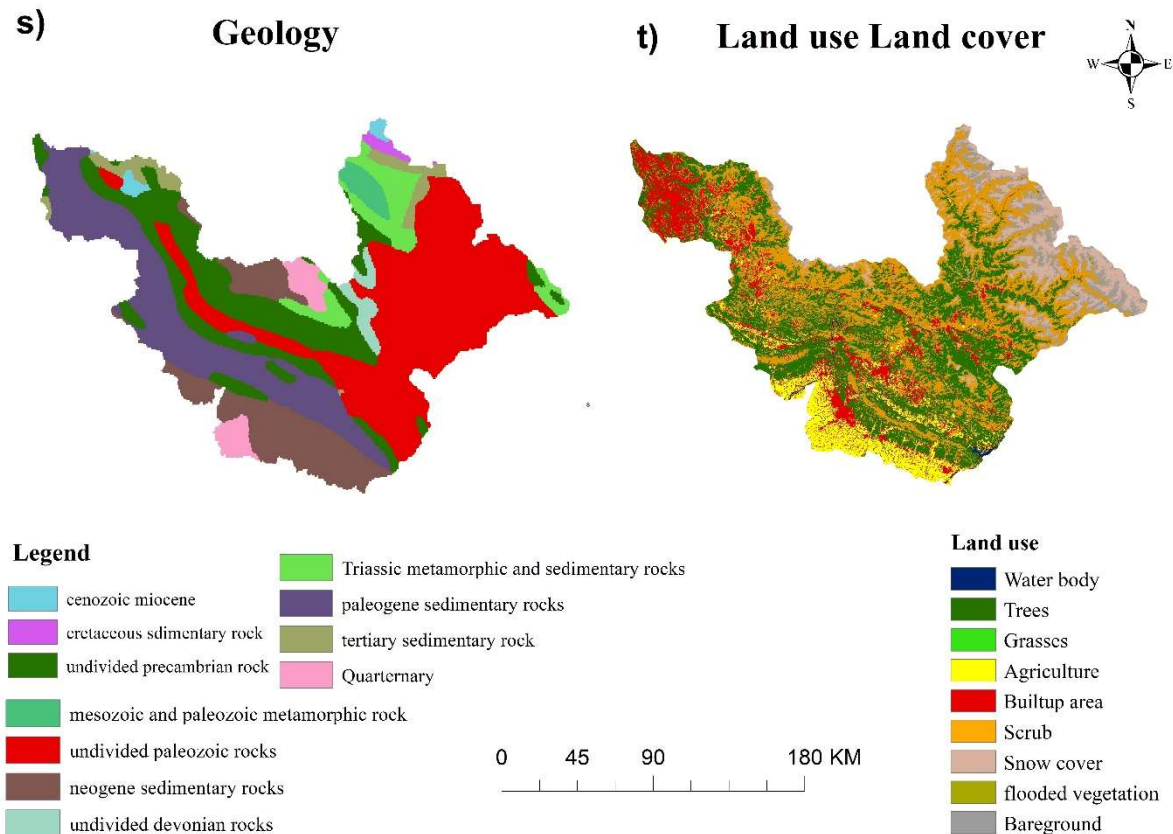


Figure 2s-2t. Geology (USGS), Land use & Land cover (drawn from Senitel-2)

Elevation: Elevation is a crucial factor in hazard monitoring, especially for earthquakes, floods, landslides, forest fires and soil erosion (Khatakho et al., 2021; Aydin et al., 2022; Nsangou et al., 2022; Intarawichian et al., 2010; Lamat et al., 2021; Aksha et al., 2020). The elevation is prepared from the extraction of the Digital Elevation Model (DEM) of Cartosat-1 (in short CARTODEM whose resolution is 30 m) downloaded from BHUVAN, a web portal of the National Remote Sensing Center (NRSC), Government of India (Figure 2r). The risk of soil erosion and landslide is not pronounced much at lower elevations whereas floods have more susceptibility at lower elevations (Gigovic et al., 2017). Often, forest fires have also been found to be decreasing with declining elevation (Rothermal et al., 1983; Lamat et al., 2021).

Evapotranspiration: Higher evapotranspiration increases drought susceptibility (Palachaudhari & Biswas, 2016). The data regarding evapotranspiration is derived from Moderate Resolution Imaging Spectroradiometer (MODIS) downloaded from United States

Geological Survey (USGS) Earth Explorer which is in gridded form for the last 10 years. Using cell statistics, mean evapotranspiration is calculated as shown in (Figure 2o).

Land Use & Land Cover: Land use & Land cover has a considerable impact on geological stability and hydrological functions which in response significantly influences all the hazards (Khatakho et al., 2021; Aksha et al., 2020; Azarafza et al., 2021; Kumar et al., 2018; Swain et al., 2020). This study prepared the land use land cover from Sentinel -2 image whose resolution is 10 m downloaded from USGS Earth Explorer (Figure 2t). The supervised classification technique using a maximum likelihood classifier is applied for preparing land use land cover in which classes are identified using Environmental System Research Institute (ESRI) classification.

5.3 Research Methodology

The present study has been performed by following three steps:

5.3.1 Preparation of Thematic Layers of Causative Factors

As discussed in the above section, all the causative factors have been processed in ArcGIS (it is discussed in 5.2 section) and their thematic layers have been prepared.

5.3.2 Finalisation of Criteria and Assignment of Weight Using AHP

The present study uses AHP for the evaluation of relative weight of conditioning factors and preparation of a pairwise comparison matrix for finalising weights of each layer for different hazards (Khezri et al., 2017; Aksha et al., 2018; Seejata et al., 2018; El Jazouli et al., 2017; Rasooli et al., 2018). The flow chart of methodology is shown in Figure 3. The existing literature showed that AHP in integration with GIS has proven an effective approach to monitoring disasters, especially, hazard mapping (Morales & de Vries, 2021). AHP is a decision-making technique developed by Saaty in the 1980s which breaks the problem into hierarchy structure and incorporated expert participation explicitly (Saaty, 2008). In this method, the objective is kept at the top, and criteria and sub-criteria followed by alternatives are placed in descending order. Further, a pairwise comparison table is prepared based on the importance scale (as given by Saaty, Table 4) and consistency index (1) and the consistency ratio (2) is computed to check the accuracy of the applied method (Saaty, 2008):

$$\text{Consistency index, (CI)} = \frac{\lambda_{max}-1}{n-1} \quad (1)$$

$$\text{Consistency ratio, (CR)} = \text{CI/RI} \quad (2)$$

whereas RI is the random index (shown in Table 5).

Table 4. Saaty’s relative importance scale (Saaty, 2008)

S. no.	Explanation	Intensity of relative Importance
1	If criteria A and B are equally important	1
2	If criteria A is moderately important than B	3
3	If criteria A is strongly important than B	5
4	If criteria A is very strongly important than B	7
5	If criteria A is extremely important than B	9
6	for intermediate judgements	2,4,6,8

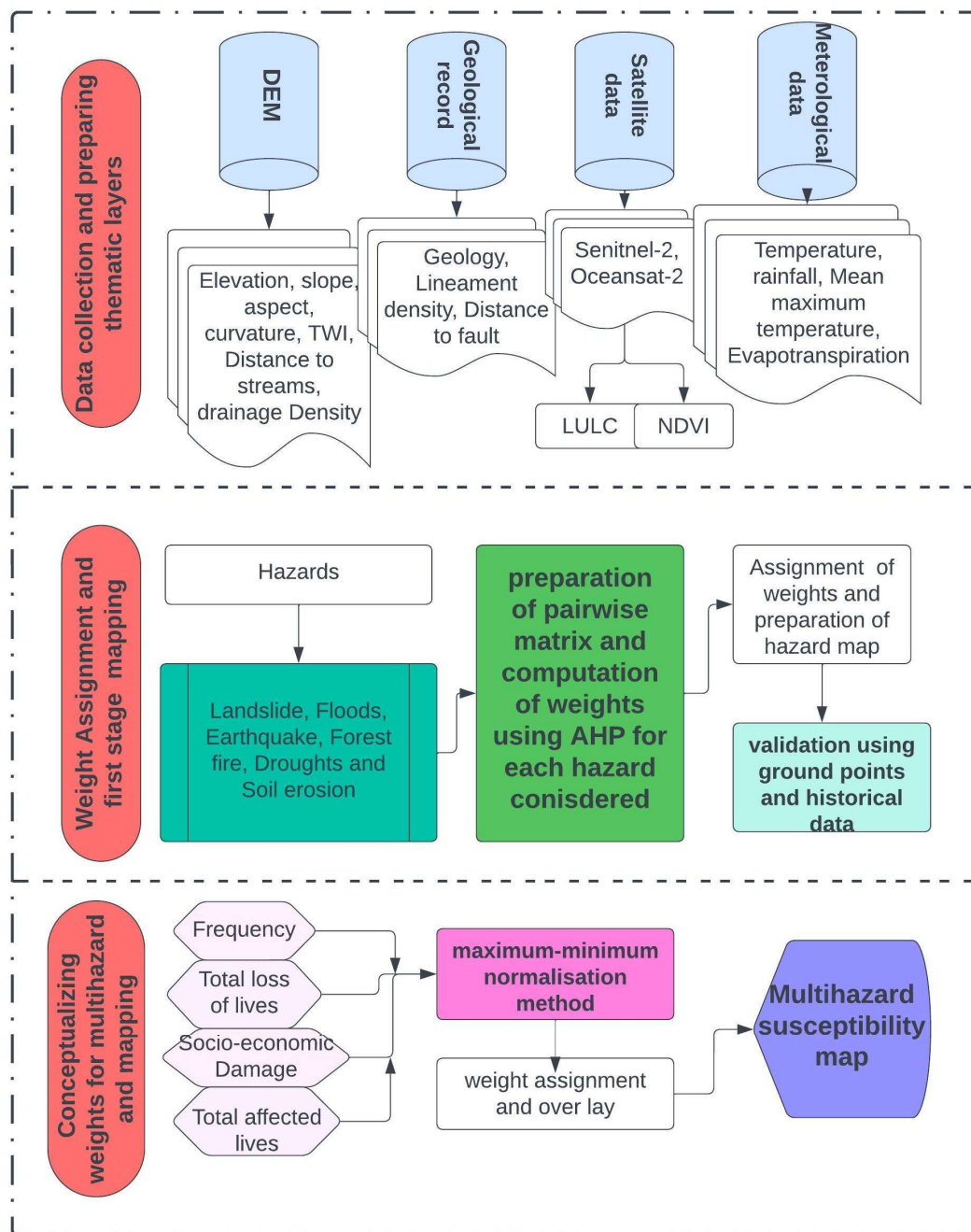


Figure 3. Flowchart of methodology followed for the present study

Table 5. Random Index provided by Saaty

N	1	2	3	4	5	6	7	8	9	10	11	12
RI	0	0	0.52	0.89	1.12	1.26	1.36	1.41	1.46	1.49	1.52	1.54

The permissible limit of CR is considered to be below 0.10 whereas some researchers accept the criteria to be 0.15 (Morales & de Vries, 2021). Moreover, when weights are evaluated, classes are also ranked on an importance scale of 1 to 9 according to the relationship between hazard and conditioning factors.

5.3.3 Overlay analysis and mapping of hazard

After the finalisation of criteria and weight, a single hazard map has been prepared after integrating the conditioning factors using the Weighted overlay tool in the ArcGIS software whose equation (3) is as follows:

$$H_i = \sum_{i=1}^n \sum_{j=1}^n (W_i * X_j) \quad (3)$$

whereas H_i is the single hazard map, W_i is the normalised weight of the i th factor and X_j is the normalised weight of the j th parameter. The computed values have been classified into five classes: very low, low, medium, high, and very high. At last, all the single hazards have been integrated into a multi-hazard map using weight (4):

$$MH = \sum_{i=1}^n w_i * H_i \quad (4)$$

whereas MH= multi-hazard and w_i = weight decided based on frequency, total affected lives, total deaths and total socioeconomic damage.

Every single hazard map is validated using historical events, and existing data available on government websites.

6. RESULTS AND DISCUSSION

6.1 Flood Hazard Assessment

To assess flood susceptibility, eleven factors have been selected and their pairwise comparison matrix is shown in Table 6. Amongst all the factors, the most influencing factors to flood hazards are found to be rainfall, distance to stream, slope, drainage density and flow accumulation as their respected normalised weights are 21%, 25%, 11%, 12% and 9% respectively. The method is consistent as the consistency ratio is found to be 0.10. the flood susceptibility map (shown in Figure 4a) is categorised into five classes: very low, low, moderate, high and very high. It is observed that 47.91 % of the area is under the moderate

zone followed by high (26.91%) and low susceptibility zone (12.88%). Southern and southwestern parts of the area are found to have a high probability of flood occurrence which may be attributable to low elevation and high rainfall in conjunction with high drainage density and proximity to distance to stream. Areas with low elevation and high drainage density have a predisposition to low infiltration and high runoff which leads to flooding (Kaledje et al., 2019; Shekhar & Pandey, 2015). Areas in the northern and northeastern parts of the area of interest are observed to have a higher probability only where there is high flow accumulation and less distance to the stream. Topographically, the northern and northeastern side of the region constitutes parts of hilly areas (above 3000m as shown in Figure 2q) that receive rainfall during the summer season but the presence of steep to precipitous slope has caused accumulation in river valleys. Thus, these parts are prone to floods near river valleys (Aksha et al., 2020). In the central part of the study area, vegetative slopes restrict the speed and amount of runoff, thus are moderately susceptible to floods (Yalcin & Akyurek, 2004). Ullah and Zhang (2020) also reported the flood occurrence near the river valley and in the areas where flat curvature, high drainage density and high TWI is found. Similar results have been observed in the study.

Table 6. Pairwise comparison table of causative factors of floods

	FL	SL	EL	DD	LULC	G	RF	DTS	TWI	C	S	NW
FL	1.00	0.33	7.00	1.00	5.00	3.00	0.14	0.20	3.00	3.00	5.00	0.09
SL	3.00	1.00	4.00	0.33	3.00	5.00	0.33	0.20	5.00	7.00	3.00	0.11
EL	0.14	0.25	1.00	0.33	3.00	0.33	0.17	0.14	0.20	2.00	3.00	0.03
DD	1.00	3.00	3.00	1.00	7.00	5.00	0.20	0.33	5.00	2.00	5.00	0.12
LULC	0.20	0.33	0.33	0.14	1.00	0.20	0.14	0.17	0.20	0.33	3.00	0.02
G	0.33	0.20	3.00	0.20	5.00	1.00	0.33	0.14	3.00	3.00	4.00	0.06
RF	7.00	3.00	6.00	5.00	7.00	3.00	1.00	0.50	6.00	6.00	5.00	0.21
DTS	5.00	5.00	7.00	3.00	6.00	7.00	2.00	1.00	5.00	5.00	7.00	0.25
TWI	0.33	0.20	5.00	0.20	5.00	0.33	0.17	0.20	1.00	3.00	0.33	0.05
C	0.33	0.14	0.50	0.50	3.00	0.33	0.17	0.20	0.33	1.00	2.00	0.03
S	0.20	0.33	0.33	0.20	0.33	0.25	0.20	0.14	3.00	0.50	1.00	0.03

Whereas, FL= Flow accumulation, SL=slope, EL=elevation, DD=drainage density, G=geology, LULC=land use land cover, RF=mean annual rainfall, DTS= distance to stream, TWI=topographic wetness index, C= Curvature, S=soil, NW= normalised weights

6.2 Earthquake Hazard Assessment

To perform earthquake hazard assessment in a GIS environment, we selected five factors as mentioned in Aksha et al., 2020 whose relative weights are shown in Table 7. This method is reliable as its consistency ratio is found to be 0.09 which is less than the threshold value. The most dominating factors are geology (24%) and distance from fault (56%). Flow accumulation has also been observed to influence seismic hazards as it enhances the chances of liquefaction by bringing unconsolidated sediments (Theilen-Willige, 2010). Five classes have been identified: very low, low, moderate, high and very high in the earthquake hazard map (Figure 4b). About 38.35% of the region falls under the very high susceptible zone

whereas a moderate susceptibility zone accounts for 33.51% followed by the high zone (23.19%). It comes to notice that the southern part of the area, which topographically lies below 300m elevation and forms part of plains have found to be under low and moderate susceptibility. Except for the southern part, the whole of the area is noticed to be under very high and high susceptibility. It is due to proximity to faults as two Faults-Main central thrust (MCT) and Main boundary thrust (MBT) lie central to the region. Though the region falls under Indian Meteorological Department (IMD) IV and V seismic zone, from the studies it is also observed that the region is highly susceptible to the earthquake (Sharma et al., 2013). Away from the fault, declining trend is noticed but comes within the 50 km range of faults which is noticed from the Figure 2a. The weak lithology of Shivalik may be another reason in the region that increases the susceptibility to the earthquake. Due to high elevation in central parts and its neighbourhood, secondary effects of earthquakes viz liquefaction, mass movements are likely to intensify the risk of impacts by an earthquake (Dhar et al., 2017).

Table 7. Pairwise comparison matrix of causative factors of earthquake

	G	DTF	FL	SL	EL	NW
G	1.00	0.20	3.00	7.00	8.00	0.24
DTF	5.00	1.00	6.00	7.00	7.00	0.56
FL	0.33	0.17	1.00	5.00	3.00	0.11
SL	0.14	0.14	0.20	1.00	1.00	0.04
EL	0.13	0.14	0.33	1.00	1.00	0.04

Whereas, G=geology, DTF=distance to fault, FL=flow accumulation, SL=slope, EL=elevation, NW=normalised weight

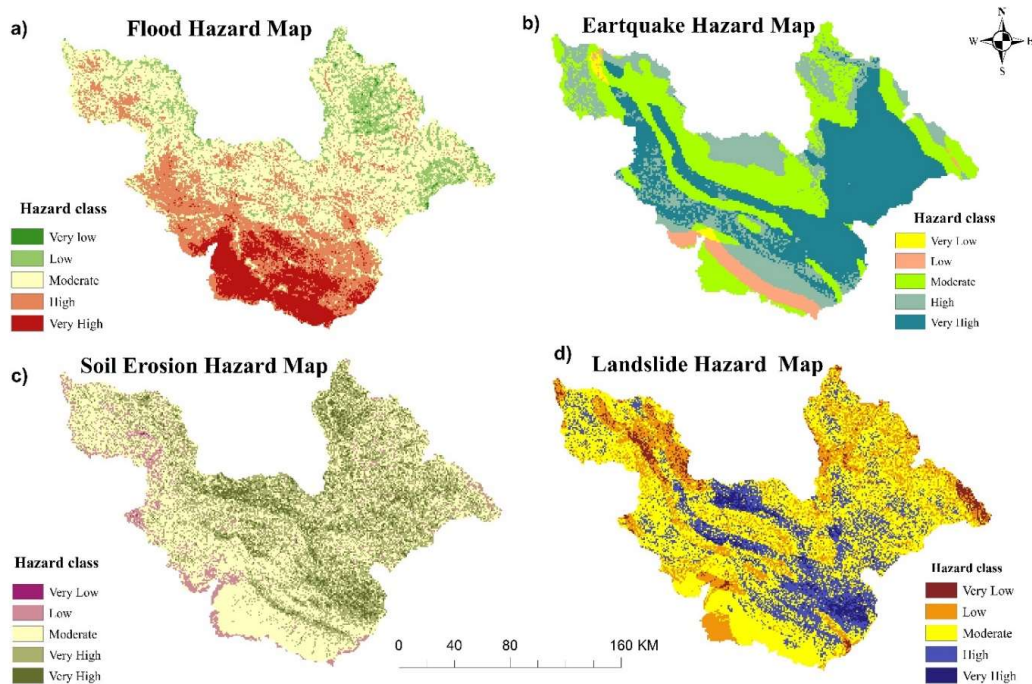


Figure 4a-4d. Flood hazard Map (4a), Earthquake hazard map (4b), Soil erosion map (4c), Landslide hazard map (4d)

6.3 Soil Erosion Hazard Assessment

In the case of soil hazard, pairwise comparison matrix of 9*9 parameters (as shown in Table 8) revealing normalised weights for the respective parameters is prepared and reliability is validated by consistency ratio whose value is $0.09 < 0.1$. Out of all the factors, slope (22.69%), Rainfall (17.15%), elevation (12%), lineament density (9.4), and Land use land cover (9.7%) are major governing factors. All the nine factors are combined using the weighted overlay tool in ArcGIS to prepare a soil erosion susceptibility map (Figure 4c). Five susceptibility classes are produced using the Natural Jenk method of classification: very low, low, moderate, high, and very high. It is deduced from the map that 34.27% of the study area is highly susceptible to soil erosion whereas only 8.14% of the area is classified under very low and low susceptible zone. Approximately half of the area is moderately exposed to soil erosion hazards. The central, southeastern, eastern and northeastern parts lie in the hilly area and are, thus, observed to have classified under the high and very high susceptible zone. In this hilly region, slopes with less vegetation and barren land are more subjected to face soil erosion. In the southern area where plain areas are found, susceptibility to soil erosion is quite low. Thus, elevation coupled with slopes and vegetative cover plays an important role in enhancing the risk of soil erosion which is further escalated by rainfall (Ebhuoma et al., 2021). Poor vegetation has a high tendency of runoff which in response increases the sediment carrying capacity (Khan et al., 2016). Curvature has also been noticed to be the main determinant in enhancing soil erosion as convex curvature is found in areas of high susceptibility zone (Aslam et al., 2021).

Table 8. Pairwise comparison for causative factors of soil erosion hazard

	LULC	NDVI	RF	EL	SL	DD	C	G	LD	NW
LULC	1.00	1.00	0.33	1.00	0.33	1.00	2.00	4.00	1.00	0.097
NDVI	1.00	1.00	0.50	0.33	0.20	0.50	1.00	3.00	0.33	0.064
RF	3.00	2.00	1.00	1.00	1.00	3.00	1.00	5.00	3.00	0.172
EL	1.00	3.00	1.00	1.00	0.33	3.00	2.00	3.00	1.00	0.128
SL	3.00	5.00	1.00	3.00	1.00	5.00	1.00	5.00	3.00	0.227
DD	1.00	2.00	0.33	0.33	0.20	1.00	0.33	2.00	0.33	0.058
C	0.50	1.00	1.00	0.50	1.00	3.00	1.00	5.00	1.00	0.116
G	0.25	0.33	0.20	0.33	0.20	0.50	0.20	1.00	2.00	0.045
LD	1.00	3.00	0.33	1.00	0.33	3.00	1.00	0.50	1.00	0.094

Whereas, SL=slope, EL=elevation, DD=drainage density, G=geology, LULC=land use land cover, RF=mean annual rainfall, LD= lineament density, NDVI= normalised difference vegetation index, C= Curvature, NW= normalised weight

6.4 Landslide Hazard Assessment

To prepare Landslide susceptibility zones, ten conditioning factors are considered as displayed in Table 9. A pairwise comparison matrix revealed that rainfall, slope, lineament density and geology are found to be major controlling factors whose relative contributing

weights are 22%, 20%,18% and 17% respectively. All factors have been superimposed to generate a Landslide Susceptibility Map as displayed in Figure 4d. Five classes are created using Natural Jenk methods-very low, low, moderate, high and very high. As determined by the consistency ratio which is 0.105, the method is reliable. The perusal of the map highlights that the maximum part of the area is under the moderate susceptibility zone which accounts for 51.22% of the total geographical area followed by high susceptibility (21.96%) and low susceptibility zone. The dominance of higher susceptibility toward landslides is observed in the central part and southeastern part whereas the southern part having a gentle slope are devoid of landslide. In the central part, rainfall received is comparatively less than in plain areas in the southern part, however, conjunction with high lineament density and the precipitous slope has increased the region’s proneness to landslide. Rainfall is, indeed, the main triggering factor (Long et al., 2018; Azarafza, 2021) but the presence of slope and geology in the region have proven to be the main causative factor in the occurrence of landslides. Region of high and very high susceptibility lies in the area having sedimentary rocks of Neogene and Paleogene rocks and undivided palaeozoic and Precambrian rocks are also present. Though the percentage share of the high and very high susceptible zone is less, the risk of landslide is enhanced due to human-induced cutting of rock for construction which is accelerated by rainfall and naked slopes (Fayaz et al., 2020). In the northeastern part, low to moderate risk has been observed whereas high risk is scattered and found along the slopes devoid of vegetation. Low risk in north eastern part may be due to the presence of snow-clad mountains where the risk of an avalanche may prevail.

Table 9. Pairwise comparison matrix of causative factors of landslide

	GE	LD	SL	EL	LULC	RF	A	S	NDVI	DTS	NW
G	1.00	0.50	2.00	6.00	4.00	0.33	5.00	5.00	5.00	3.00	0.17
LD	2.00	1.00	2.00	5.00	4.00	0.33	6.00	4.00	4.00	4.00	0.18
SL	0.50	0.50	1.00	5.00	4.00	4.00	6.00	4.00	5.00	5.00	0.20
EL	0.17	0.20	0.20	1.00	0.20	0.20	2.00	0.33	0.33	0.50	0.03
LULC	0.25	0.25	0.25	5.00	1.00	0.20	2.00	0.33	2.00	3.00	0.06
RF	3.00	3.00	0.25	5.00	5.00	1.00	4.00	5.00	5.00	5.00	0.22
A	0.20	0.17	0.17	0.50	0.50	0.25	1.00	0.33	0.33	0.50	0.02
S	0.20	0.25	0.25	3.00	3.00	0.20	3.00	1.00	0.50	3.00	0.06
NDVI	0.20	0.25	0.20	3.00	0.50	0.20	3.00	2.00	1.00	2.00	0.05
DTS	0.33	0.25	0.20	2.00	0.33	0.20	2.00	0.33	0.50	1.00	0.04

Whereas SL=slope, EL=elevation, DD=drainage density, G=geology, LULC=land use land cover, RF=mean annual rainfall, LD= lineament density, NDVI= normalised difference vegetation index, A= aspect, DTS= distance to stream, NW= normalised weight

6.5 Droughts Hazard Assessment

GIS-based drought assessment in combination with AHP has proven to be effective in hazard monitoring (Palachaudhari & Biswas, 2016; Ying et al., 2007). In this study, nine factors have been selected and normalised weights are shown in Table 10. Their weights are

further used as an input while overlaying layers in GIS to prepare the Droughts Hazard Susceptibility map (Figure 4e). Mean annual temperature, mean maximum temperature, rainfall, evapotranspiration and relative humidity according to their corresponding weight viz 23.36%, 21.97%, 17.56%, 15.03%, 10.3% are observed to have an impact the drought susceptibility. The AHP method is reliable as per the results of the consistency ratio which comes out to be 0.09 less than Saaty’s threshold. The map indicates that the region tends to face drought because 44.57% of the area is covered by a highly susceptible zone which is followed by a moderate risk zone (35.23%). In southern plains where lack of vegetation, high agricultural land, high mean maximum temperature, and low to moderate evapotranspiration have increased the likelihood of drought occurrence despite no such event has been experienced so far. Shortage of rainfall causes drought and maximum high temperature induced high evapotranspiration to create a drought-like condition in an agricultural area (Basu et al., 2015; Palachaudhari & Biswas, 2016). Northeastern and central hilly areas fall under moderate and high drought risk zone due to perennial snow-covered mountains, barren land and high evapotranspiration (Basu et al., 2015). Low susceptible zones are found in the central northern part mainly due to moderate rainfall, moderate evapotranspiration and highly vegetative slopes. The western part of the area shows a likelihood of a high level of drought hazard.

Table 10. Pairwise comparison matrix of causative factors causing drought

	RF	T	Tmax	ET	RH	S	LULC	SL	NDVI	NW
RF	1.00	0.20	0.50	3.00	2.00	6.00	6.00	8.00	9.00	0.176
T	5.00	1.00	0.50	1.00	2.00	6.00	6.00	8.00	9.00	0.234
Tmax	2.00	2.00	1.00	1.00	3.00	6.00	6.00	8.00	6.00	0.220
ET	0.33	1.00	1.00	1.00	2.00	6.00	6.00	8.00	3.00	0.150
RH	0.50	0.50	0.33	0.50	1.00	6.00	6.00	8.00	3.00	0.109
S	0.17	0.17	0.17	0.17	0.17	1.00	0.50	4.00	2.00	0.032
LULC	0.17	0.17	0.17	0.17	0.17	2.00	1.00	2.00	4.00	0.037
SL	0.13	0.13	0.13	0.13	0.13	0.25	0.50	1.00	2.00	0.020
NDVI	0.11	0.11	0.17	0.33	0.33	0.50	0.25	0.50	1.00	0.022

Whereas, SL=slope, ET=evapotranspiration, Tmax=mean maximum temperature, G=geology, LULC=land use land cover, RF=mean annual rainfall, RH=relative humidity, NDVI= normalised difference vegetation index, S=soil, NW= normalised weight

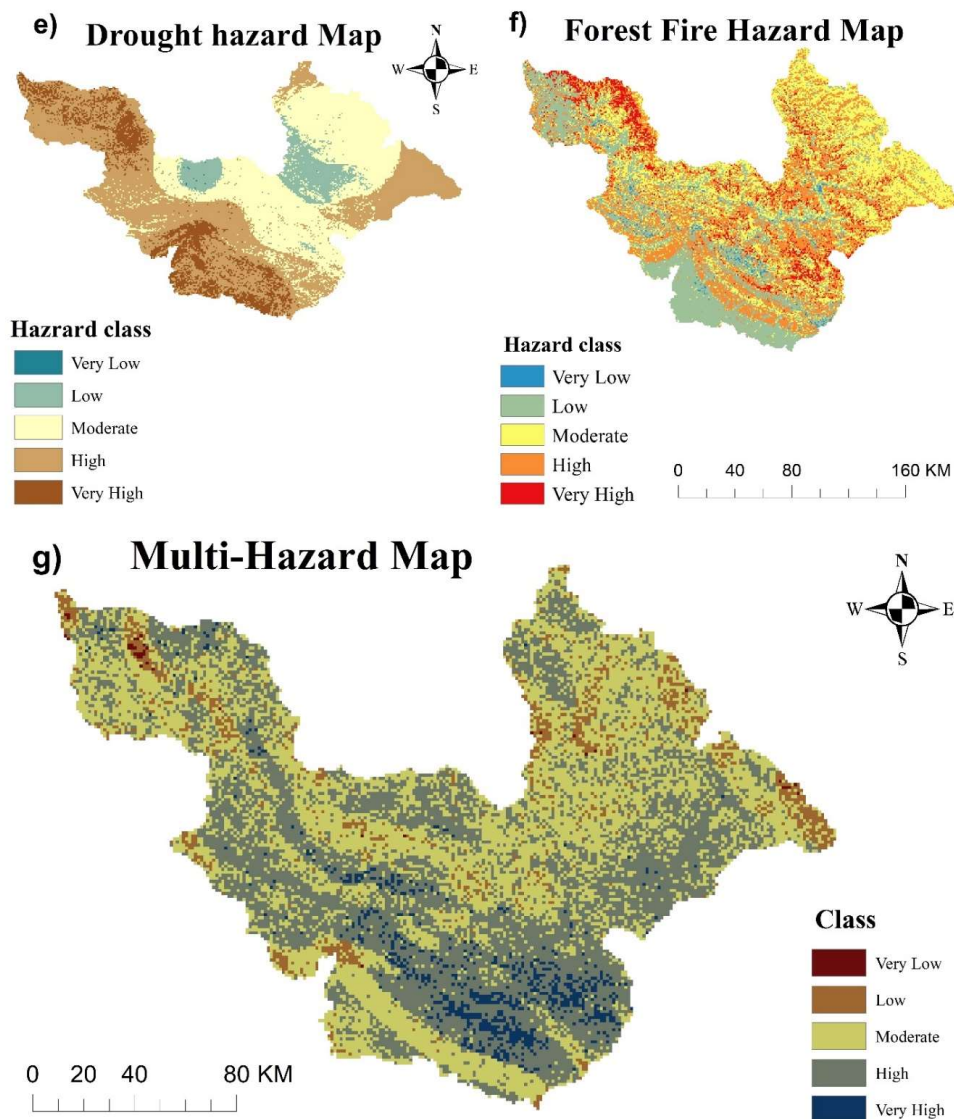


Figure 4e-4g. Drought hazard map (4e), Forest fire hazard map (4f), Multi-hazard map (4g)

6.6 Forest Fire Hazard Assessment

Forest fire incidents are common in forest areas, especially during the summer season, which motivate to perform forest fire hazard assessment. The GIS-based environment in integration with AHP has provided us simplified approach to evaluate the risk of occurrence of a forest fire. Seven factors have been shortlisted whose pairwise matrix of 7x7 is displayed in the Table 11. The feasibility of the method can be checked by the consistency ratio which is $0.065 < 0.1$. The map (Figure 4f) depicts that only 32.08% area is under a highly susceptible zone. Nearly 32.87% area falls under the moderate susceptible zone. Low susceptibility area to forest fire accounts for 26.9%. Elevation (21%), Land use land cover (36%), and temperature (18%) have been observed to put the maximum influence on fire occurrence. There are no well-defined zones noticed on the map. However, the southern plains having a

higher share of agricultural land is less susceptible to fire incidents despite the fact it receives maximum temperature compared to other areas. High to very high susceptibility is observed in vegetative slopes in the central and western parts of the region as vegetation density influences the amount of fire (Rasooli et al., 2018). In the eastern part, moderate susceptibility is noticed mainly due to the presence of shrub-laden slopes, and low temperature. Wind speed affects generally the spreading of the fires and enhances the intensity (Cruz & Alexander, 2019).

Table 11. Pairwise comparison of causative factors causing forest fire

	T	RF	WS	LULC	EL	SL	A	NW
T	1.00	6.00	4.00	0.33	0.50	3.00	4.00	0.18
RF	0.17	1.00	0.33	0.20	0.20	0.33	0.33	0.03
WS	0.25	3.00	1.00	0.20	0.20	0.33	0.33	0.05
LULC	3.00	5.00	5.00	1.00	3.00	4.00	5.00	0.36
EL	2.00	5.00	5.00	0.33	1.00	2.00	4.00	0.21
SL	0.33	3.00	3.00	0.25	0.50	1.00	2.00	0.10
A	0.25	3.00	3.00	0.20	0.25	0.50	1.00	0.07

Whereas, T=temperature, RF= mean annual rainfall, WS=wind speed, LULC= land use land cover, SL=slope, EL= elevation, A=aspect, NW=normalised weights

6.7 Multi-hazard Assessment

After overlaying all the hazards, a multi-hazard map is generated (Figure 4g) which reveals region susceptibility to multiple hazards. Five categories were generated using the Natural Jenk classification method to demonstrate which part of the area is more susceptible to multi-hazards. It is depicted from the map that 45.79% of the area is prone to moderate susceptibility whereas 43.43% of the region is predisposed to high susceptibility. Low susceptibility is found in only 6.72% of the area. Interestingly, the central and eastern parts of the region are close to faults and weak lithology is dominated by a high level of multi-hazards. The Southern plain area is susceptible to moderate levels of multi-hazard. Increasing urbanisation in the southern part (Figure 2t) may also escalate the risk of multi-hazards.

Table 12. Weights showing the influence of hazard in multi-hazard susceptibility

S. No.	Hazard	Weight
1	Flood	28
2	Landslide	18
3	Earthquake	18
4	Drought	15
5	Forest Fire	13
6	Soil Erosion	11

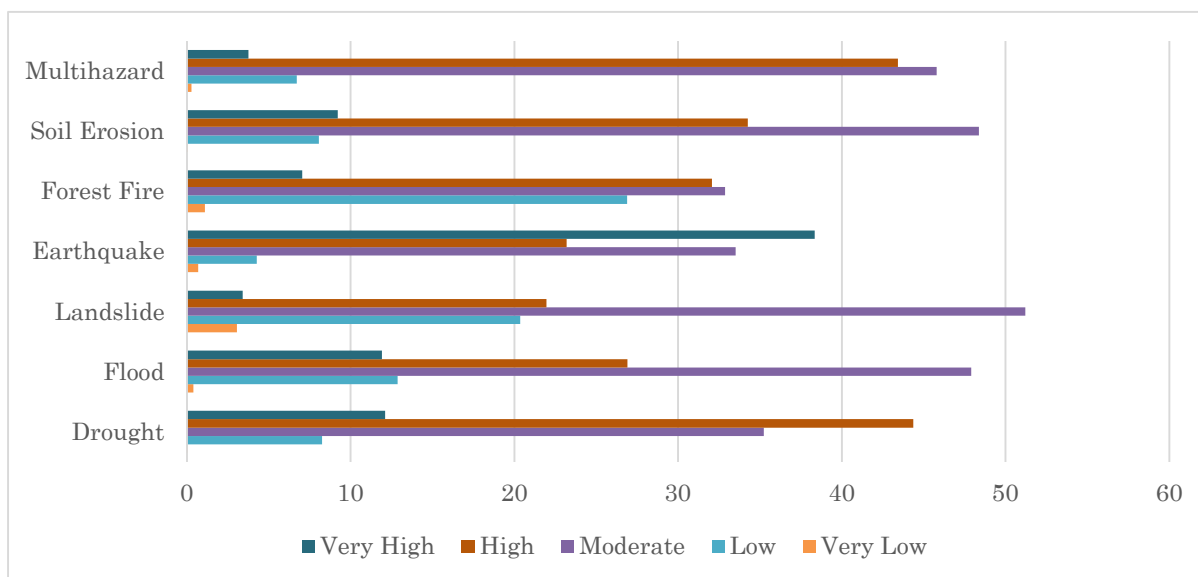


Figure 5. Percentage wise area covered by each hazard in each susceptibility zone

6.8 Validation

Every work lack justification until it is verified. Keeping this in consideration, landslide and earthquake hazard maps are validated using the historical incidents in the point form downloaded from the Bhukosh, web-portal of Geological Survey of India which showed that maximum incidents are superimposed on high and very high susceptible zones. For validating flood hazard map, 250 points are generated from visual interpretation of Google Earth image. 82.17% of the total points lie on high and moderate susceptible zone. Forest fire map is validated using fire points produced by Forest Survey of India. For droughts, Indian Meteorological Department (IMD) hazard atlas is utilised and it is observed that high susceptible region in our study area falls under IMD’s moderate drought zone.

6.9 Discussion

The results of the study indicated the assessment of the “Hazard” component of the UNDRR Risk Framework. The study revealed the multi-hazard susceptibility map of the study area as Nachappa (2020) stated that emphasis on single hazards is constructive but if an area is susceptible to multiple-hazards then potential danger should be considered from all the hazards despite only one. The present work provided a map that represents multiple threats from natural hazards dominantly covering six geo-hydrological hazards as per the geophysical condition of the area. The multi-hazard map is prepared by considering 20 natural stable and triggering factors whose mere presence increases the likelihood of the occurrence of hazards. The multi-criteria Analytical Hierarchy Process (AHP) played a dominant role and proved to be beneficial for combining the different factors in a multi-hazard susceptibility map (Rahmati et al., 2019; Khatakho et al., 2021). Though this method is subjective in weighing criteria, we can enhance objectivity with literature and expert

involvement. Similarly, this method is appreciated by Morales and de Vries (2021). Multitudes of studies (Aksha et al., 2020; Khatakho et al., 2021; Morales & de Vries, 2021) have applied AHP to prepare a multi-hazard susceptibility/exposure map. The other studies on multi-hazard mapping have promoted machine learning and deep learning techniques but utilization of such techniques usually involved greater complexities and sophisticated technology (Poyan et al., 2021; Javidan et al., 2020; Ullah et al., 2022). It is pertinent to mention that no study has so far been conducted to involve AHP in more than four hazards as this study. The study is unique in finding weightage quantitatively using maximum and minimum normalisation method for individual hazards by utilizing the historical frequency and damages caused by hazard.

The results indicated that rainfall, curvature, TWI, flow accumulation and drainage density have a substantial impact on floods affecting 61% of the study area which is evidenced by the work of Pourghasemi et al. (2020) and Pujari and Wayal (2023) who mentioned the occurrence of flooding in flat areas, coupling discharge accumulation and low runoff. Around 43% of study area is affected by high soil erosion risk which is enhanced by mainly vegetation with less slope, high rainfall, and convex slopes. The work of Saini et al. (2015) and El Jazouli et al. (2017) also shows similarity. As far as landslides are concerned, geology, rainfall, slope, and lineament density are the main causative factor affecting 75% of the area which can also be observed in Dou et al., 2020; Fang et al., 2021; Khatakho et al. (2021). In the case of drought, evapotranspiration, maximum temperature, rainfall, and elevation make 56% of the region susceptible as if any shortage in rainfall and excessive deforestation can turn out to be havoc for the study area. Singh et al. (2017) justified the drought event using the tree ring method which showed the 1780s to be the driest period for the North-western Himalayas which turns out to be the eastern part of the study area. The presence of the Kandi belt in the southern part that spans over three districts has a high propensity to droughts as Kumar et al. (2004) mentioned this area as a water-scarce region. Around 43% of the study area fall under critical forest fire region which is influenced by temperature, vegetative cover, and elevation. Gheshlaghi et al. (2020) and Rasooli et al. (2018) also showed similar results. From the final map, it is noticed that 43.43% of the area has a high propensity to suffer from multi-hazards. The area under the high susceptibility class lies close to faults and weak lithology as the distance to faults and geology reflected.

The present study attempted to prioritize the high and very high susceptibility zones for further disaster risk management. This will facilitate in identification of communities and capacitating them being resilient to future challenges from these mishaps. This prioritization will further aid in minimizing the future impacts by adopting proactive measures, reducing individual financial burden and allocating resource during any disaster since these zones have higher probability of experiencing threat from multiple hazards.

The limitation of the study is that there may be more space for additional factors to be used in the individual hazard assessment that can be utilised to elevate the impact of the study. The new methods like random forest, machine learning and convolutional neural network

methods have the ability to show an interaction between hazards which this study lacks. This study requires upscaling and downscaling of the data that have the ability to exaggerate the resolution of thematic layers. Utilising the final outcome of the study, suitable measure such as strengthening the capacity building measure, slope regeneration (on the construction site), awareness campaign, and providing disaster mitigation kit related information should be adopted for disaster risk reduction in the prioritized susceptibility zones. The future risk studies should be conducted in the study area on district scale for more accurate prediction of the hazards.

7. CONCLUSION

Multi-hazard susceptibility mapping is becoming popular and becoming state-of-the-art approach in disaster management. Having a predilection towards the multiple threats, prioritization for disaster risk management is crucial for resource allocation, reducing vulnerabilities and fostering risk reduction. The insights from the study highlighted that more than 70% of the area is predisposed to moderate and high levels of susceptibility. The central part and adjoining areas near faults should be given attention from the context of multi-hazards. By comprehending the prioritized zones, we can build safer and more resilient communities capable of withstanding the challenges caused by multi-hazard. It is in response to these zones adaptive capacity of communities can be enhanced by proactive measures and comprehensive planning and targeted intervention by stakeholders to be undertaken for disaster risk reduction.

ACKNOWLEDGEMENTS

The authors would like to thank National Remote Sensing Centre (NRSC), United States Geological Survey (USGS), National Aeronautics, Space Administration (NASA), Climate research Unit (CRU), Geological Survey of India (GSI), Moderate Resolution Imaging Spectroradiometer (MODIS) and Global Wind Atlas for providing necessary data in smooth functioning of the project. The authors also would like to thank their supervisor and IOE, BHU for providing technical support to work on the related topic.

CONFLICT OF INTEREST

Authors don't have any conflict in authorship

REFERENCES

- Adab, H., Kanniah, K., & Solaimani, K. (2013). Modeling forest fire risk in the northeast of Iran using remote sensing and GIS techniques. *Natural Hazards*. 65(3):1723– 1743.

- Aksha, S. K. (2018). *Assessing vulnerability and multi-hazard risk in the Nepal Himalaya* [Doctoral dissertation, Virginia Tech].
- Aksha, S., Resler, L., Juran, L., & Carstensen, Jr. W. (2020). A geospatial analysis of multi-hazard risk in Dharan, Nepal. *Geomatics, Natural Hazards and Risk*, 11:1, 88- 111, <https://doi.org/10.1080/19475705.2019.1710580>
- Ali, N., Alam, A., Bhat, M. S., & Shah, B. (2022). Using historical data for developing a hazard and disaster profile of the Kashmir valley for the period 1900–2020. *Natural Hazards*, 114(2), 1609-1646.
- Althuwaynee, O., Pradhan, B., Park, H.J., & Lee, J. H. (2014). A novel ensemble bivariate statistical evidential belief functions with knowledge-based analytical hierarchy process and multivariate statistical logistic regression for landslide susceptibility mapping. *Catena*, 114:21–36.
- Angeli, S., Malamud, B., Rossi, L., Tylor, F., Trasforini, E., & Rudari, R. (2022). A multi-hazard framework for spatial-temporal impact analysis. *International Journal of Disaster Risk Reduction*, 73, 102829. <https://doi.org/10.1016/j.jidrr.2022.102829>
- Arulbalaji, P., Padmalal, D., & Sreelash, K. (2019). GIS and AHP techniques based delineation of groundwater potential zones: A case study from Southern Western Ghats, India. *Scientific Reports*, 9, 2082. <https://doi.org/10.1038/s41598-019-38567-x>
- Aslam, B., Maqsoo, A., Alaloul, W. S., Musarat, M., Jabbar, T., & zafar, A. (2021). Soil erosion susceptibility Mapping Using a GIS-b multi-criteria decision approach: case of district Chitral, Pakistan. *Ain Shams Engineering Journal*, 12, 1637-1649. <https://doi.org/10.1016/j.asej.2020.09.015>
- Ayidin, M., & Birincioglu, E. (2022). Flood risk analysis using gis-based analytical hierarchy process: a Case study of Bitlis Province. *Applied Water Science*, 12:122. <https://doi.org/10.1007/s13201-022-01655-x/>
- Azarafza, M., Azarafza, M., Akgün, H., Atkinson, P. M., & Derakhshani, R. (2021). Deep learning-based landslide susceptibility mapping. *Scientific reports*, 11(1), 1-16.
- Basu, M., Hoshino, S., & Hashimoto, S. (2015). Many issues, limited responses: coping with water insecurity in rural India. *Water Resour Rural Dev*, 5:47–63
- Bennett, B., Leonard, M., Deng, Y., & Westra, S. (2018). An empirical investigation into the effect of antecedent precipitation on flood volume. *Journal of hydrology*, 567, 435-445.
- Berry, R.(2009). A review of the use of the Geographic information system in Hazard and disaster management. Report submitted to University of Glamorgan.
- Chandra, R., Dar, J., Romshoo, S., Rashid, I., Parvez, I., & Mir, S. et al. (2018). Seismic hazard and probability assessment of Kashmir valley, northwest Himalaya, India. *Natural Hazards*, 93, 1451–1477. doi: 10.1007/s11069-018-3362-4
- Cruz, M. G., & Alexander, M. E. (2019). The 10% wind speed rule of thumb for estimating a wildfire's forward rate of spread in forests and shrublands. *Annals of Forest Science*, 76(2), 1-11.
- Das, S. (2019). Geospatial mapping of flood susceptibility and hydro-geomorphic response to the floods in Ulhas basin, India. *Remote Sensing Applications: Society and Environment*, 14, 60-74.

- Dasanayaka, U. and Matsuda, Y. (2022). “Consensus of Local Knowledge on Landslide Hazard in Depopulated Mountain Communities in Japan – A Case Study on Matsunoyama Village.” *IDRiM Journal*, 12 (2): 1–22. <https://doi.org/10.5595/001c.55587>.
- Dhar, S., Rai, A., & Nayak, P. (2017). Estimation of seismic hazard in Odisha by remote sensing and GIS techniques. *Natural Hazards*, 86(2):695–709.
- Dou, J., Yunus, A. P., Merghadi, A., Wang, X. K., & Yamagishi, H. (2020). A comparative study of deep learning and conventional neural network for evaluating landslide susceptibility using landslide initiation zones. In *Workshop on World Landslide Forum* (pp. 215-223). Springer, Cham.
- Ebhuoma, O., Gebreslasie, M., Ngetar, N. S., Phinzi, K., & Bhattacharjee, S. (2022). Soil Erosion Vulnerability Mapping in Selected Rural Communities of uThukela Catchment, South Africa, Using the Analytic Hierarchy Process. *Earth Systems and Environment*, 1-14.
- El Jazouli, A., Barakat, A., Ghafiri, A., El Moutaki, S., Ettaqy, A., & Khellouk, R. (2017). Soil erosion modeled with USLE, GIS, and remote sensing: a case study of Ikkour watershed in Middle Atlas (Morocco). *Geoscience Letters*, 4(1), 1-12.
- Eshrati, L., Mahmoudzadeh, A., & Taghvaei, M. (2015). Multi hazards risk assessment, a new methodology. *International Journal of Health System and Disaster Management*, 3(2).
- Fang, Z., Wang, Y., Peng, L., & Hong, H. (2021). A comparative study of heterogeneous ensemble-learning techniques for landslide susceptibility mapping. *International Journal of Geographical Information Science*, 35(2), 321–347. <https://doi.org/10.1080/13658816.2020.1808897>
- Fayaz, M., & Khader, S. A. (2020). Identifying the parameters responsible for Landslides on NH-44 Jammu Srinagar National Highway for Early Warning System. *Disaster Advances*, 13(2), 32-42.
- Gheshlaghi, A. H., Feizizadeh, B., Blaschke, T., Lakes, T., & Tajbar, S. (2020). Forest fire susceptibility modeling using Hybrid approaches. *Transactions in GIS*. 25, 311-333.
- Gigović, L., Pamučar, D., Bajić, Z., & Drobnjak, S. (2017). Application of GIS-interval rough AHP methodology for flood hazard mapping in urban areas. *Water*, 9(6), 360.
- GWRA. (2020). Ground water resources of union territory of Jammu and Kashmir. Retrieved from government website of Jammu and Kashmir <https://cgwb.gov.in/>
- Harris, I., Osborn, T. J., Jones, P., & Lister, D. (2020). Version 4 of the CRU TS monthly high-resolution gridded multivariate climate dataset. *Scientific data*, 7(1), 1-18. <https://doi.org/10.1038/s41597-020-0453-3>
- Hassan R. (2014). Disasters in Kashmir: Impact and Response. *Journal of Humanities and Social Science*, 19(7):32-42.
- Hewitt, K., Burton, I. (1971). *Hazardousness of a place: a regional ecology of damaging events*. Toronto Press, Toronto
- Hoque, M., Phinn, S., Roelfsema, C., & Childs, I. (2018). Assessing tropical cyclone risks using geospatial techniques. *Applied Geography*, 98:22–33.
- IMD. (2014). Climate of Jammu and Kashmir. Indian: Indian Meteorological Department. Available from http://www.diragriju.nic.in/CSS%20GUIDELINES/FINAL_CLIMATE%20OF%20JAMMU%20AND%20KASHMIR_e%20book.pdf

- Intarawichian, N., & Dasananda, S. (2010). Analytical hierarchy process for Landslide Susceptibility mapping in Lower Mae Chaem Watershed, Northern Thailand. *Suranaree J. Sci. Technol.*, 17(3):1-16
- Javidan, N., kavian, A., pourghasemi, H. R., Conoscenti, C., Jafrian, Z., & Comino, J. (2020). Evaluation of multi-hazard map produced using MaxEnt machine learning technique. Scientific reports, 11,6496. Retrieved from www.nature.com/scientificreports/. <https://doi.org/10.1038/s41598-021-85862-7>
- Kabenge, M., Elaru, J., Wang, H., & Li, F. (2017). Characterizing flood hazard risk in data-scarce areas, using a remote sensing and GIS-based flood hazard index. *Natural Hazards*, 89(3):1369–1387
- Kalédjé, P. S. K., Ngoupayou, J. R. N., Takounjou, A. F., Zebsa, M., Rakotondrabe, F., & Ondoa, J. M. (2019). Floods of 18 and 19 November 2016 in Batouri (East Cameroon): interpretation of the hydro-meteorological parameters and historical context of the post-event survey episode. *The Scientific World Journal*, 2019.
- Kappes, M. (2011). Multi-hazard risk analyses: a concept and its implementation. PhD thesis, University of Vienna.
- Kappes, M. S., Keiler, M., von Elverfeldt, K. & Glade, T. (2012). Challenges of analyzing multi-hazard risk: A review. *Natural Hazards*, 64, 1925–1958.
- Kaur, H., Gupta, S., Parkash, S., Thapa, R., Gupta, A., Khanal, G.C. (2019). Evaluation of landslide susceptibility in a hill city of Sikkim Himalaya with the perspective of hybrid modelling techniques. *Spatial Sci.*, 25 (2), 113–132. <https://doi.org/10.1080/19475683.2019.1575906>
- Kazakis, N., Kougiass, I., & Patsialis, T. (2015). Assessment of flood hazard areas at a regional scale using an index-based approach and Analytical Hierarchy Process: application in Rhodope–Evros region, Greece. *Sci Total Environ.*, 538:555–563
- Khan, M.N., Gong, Y., Hu, T., et al. (2016). Effect of slope, rainfall intensity and mulch on erosion and infiltration under simulated rain on purple soil of south-western Sichuan province, China. *Water*, 8:528
- Khatakho, R., Gautam, D., Aryal, K. R., Pandey, V. P., Rupakhety, R., Lamichhane, S., Liu, Y.C., Abdouli, K., Talchabhadel, R., Thapa, B.R., & Adhikari, R. (2021). Multi-hazard risk assessment of Kathmandu Valley, Nepal. *Sustainability*, 13(10), 5369.
- Khezri, E., Maleknia, R., Zeinivand, H., & Badehin, Z. (2017). Mapping natural resources vulnerability to droughts using multi-criteria decision making and GIS (case study: Kashkan Basin Lorestan Province, Iran). *Journal of Rangeland Science*, 7(4), 376-386.
- Khosravi, K., Nohani, E., Maroufinia, E., & Pourghasemi, H.R. (2016). A GIS-based flood susceptibility assessment and its mapping in Iran: a comparison between frequency ratio and weights-of-evidence bivariate statistical models with multi-criteria decision-making technique. *Natural Hazards*. 83: 947–987. <https://doi.org/10.1007/s11069-016-2357-2>
- Kumar, R., & Acharya, P. (2016). Flood hazard and risk assessment of 2014 floods in Kashmir valley: a space-based multi-sensor approach. *Natural Hazards*, 84, 437–464. doi: 10.1007/s11069-016-2428-4
- Kumar, V., Gupta, V., Jamir, I. (2018). Hazard evaluation of progressive Pawari landslide zone, Satluj valley, Himachal Pradesh, India. *Natural Hazards*, 93 (2), 1029–1047. <https://doi.org/10.1007/s11069-018-3339-3>

- Kumar, V., Rai, S. P., & Rathore, D. S. (2004). Land use mapping of Kandi belt of Jammu region. *Journal of the Indian Society of Remote Sensing*, 32(4), 323-328.
- Lamat, R., Kumar, M., Kundu, A., & Lal, D. (2021). Forest fire risk mapping using analytical hierarchy process (AHP) and earth observation datasets: A case study in the mountainous terrain of Northeast India. *SN Applied Sciences*, 3(4), 1-15.
- Lehner, B., Döll, P., Alcamo, J., Henrichs, T., & Kaspar, F. (2006). Estimating the impact of global change on flood and drought risks in Europe: a continental, integrated analysis. *Climatic Change*, 75(3):273–299.
- Liu, B., Siu, Y. L., Mitchell, G., & Xu, W. (2016). The danger of mapping risk from multiple natural hazards. *Natural Hazards*, 82, 139-153.
- Long, N.T., De Smedt, F. (2018). Analysis and mapping of rainfall-induced landslide susceptibility in A luoi district, thua thien hue province. Vietnam. *Water (Switzerland)* 11 (1). <https://doi.org/10.3390/w11010051>.
- Morales, F. F. Jr., & de Vries, W.T. (2021). Establishment of Hazards Mapping Criteria Using Analytic Hierarchy Process (AHP). *Front. Sustain.*, 2:667105. doi: 10.3389/frsus.2021.667105
- Nachappa, T. G. (2020). Geoinformatics methods for Multi-Hazards Susceptibility Mapping and Assessment. A Doctoral dissertation submitted to Paris-Lodron Universität Salzburg.
- Nsangou, D., Kpoumié, A., Mfonka, Z., Ngouh, A.N., Fossi, D.H., Jourdan, C., Mbele, H.Z., Mouncherou, O.F., Vandervaere, J.P. & Ngoupayou, J.R.N. (2022). Urban flood susceptibility modelling using AHP and GIS approach: case of the Mfoundi watershed at Yaoundé in the South-Cameroon plateau. *Scientific African*, 15, e01043.
- Palachaudhuri, M., & Biswas, S. (2016). Application of AHP with GIS in drought risk assessment for Puruliya district, India. *Natural Hazards*, 84,1905-1920. doi 10.1007/s11069-016-2526-3
- Patel, S. K., Nanda, A., Singh, G., et al. (2020). A review of disasters in Jammu and Kashmir, and Ladakh region in India. *International Journal of Population Studies*, 6(1), 69-81. doi: 10.18063/ijps.v6i1.1180
- Paul, G. C., Saha, S., & Hembram, T. K. (2019). Application of the GIS-based probabilistic models for mapping the flood susceptibility in Bansloi sub-basin of Ganga-Bhagirathi river and their comparison. *Remote Sensing in Earth Systems Sciences*, 2(2), 120-146.
- Pellicani, R., Argentiero, I., & Spilotro, G. (2017). GIS-based predictive models for regional-scale landslide susceptibility assessment and risk mapping along road corridors. *Geomatics, Natural Hazards and Risk*, 8(2), 1012–1033.
- Pimentel, J., Dutra, t., Ribeiro, R.S., dos santos Pfaltzgraff, P.A., Brenny, M. E. R., Peixoto, D., da Silva, D. R., Iwanami, H., Nishimura, T. (2020). Risk assessment and hazard mapping technique in the project for strengthening national strategy of integrated natural disaster risk management. *International Journal of Erosion Control Engineering*, 13(1), pp.35-47.
- Pourghasemi, H. R., Gayen, A., Edalat, M., Zarafshar, M., & Tiefenbacher, J. P. (2020). Is multi-hazard mapping effective in assessing natural hazards and integrated watershed management?. *Geoscience Frontiers*, 11(4), 1203-1217.

- Pourghasemi, H. R., & Kerle, N. (2016). Random forests and evidential belief function-based landslide susceptibility assessment in Western Mazandaran Province, Iran. *Environmental earth sciences*, 75(3), 1-17.
- Pouyan, S., Pourghasemi, H.R., Bordbar, M., Rahmanian, S., & Clague, J. (2021). A multi-hazard map-based flooding, gully erosion, forest fires, and earthquakes in Iran. *Scientific reports*, 11, 14889. Retrieved from www.nature.com/scientificreports/. <https://doi.org/10.1038/s41598-021-94266-6>
- Psomas, A., Vryzidis, I., Spyridakos, A., & Mimikou, M. (2018). MCDA approach for agricultural water management in the context of water-energy-land-food nexus. *Oper. Res.* 21, 689–723. doi: 10.1007/s12351-018-0436-8
- Pujari, S., and Wayal, A.S. (2023). “Impact of Climate Change and Land Use Change on Coastal Areas: A Case Study Thane, India.” *IDRiM Journal* 12 (2): 23–39. <https://doi.org/10.5595/001c.74306>.
- Rahmati, O., Yousefi, S., Kalantari, Z., Uuemaa, E., Teimurian, T., Keesstra, S., ... & Tien Bui, D. (2019). Multi-hazard exposure mapping using machine learning techniques: A case study from Iran. *Remote Sensing*, 11(16), 1943.
- Rasooli, S. B., Bonyad, A. E., & Pir Bavaghar, M. (2018). Forest fire vulnerability map using remote sensing data, GIS and AHP analysis (Case study: Zarivar Lake surrounding area). *Caspian Journal of Environmental Sciences*, 16(4), 369-377.
- Rincón, D., Khan, U. T., & Armenakis, C. (2018). Flood risk mapping using GIS and multi-criteria analysis: A greater Toronto area case study. *Geosciences*, 8(8), 275.
- Rothermel, R.C. (1983). How to predict the spread and intensity of forest and Range fires. Gen Tech Rep INT-143. USDA Forest Service. Intermountain Forest and Range Experiment Station, pp 1–168.
- Saaty, T. L. (2008). Decision making with the analytic hierarchy process. *International Journal of Services Sciences*, 1, 83–98
- Saha, S., Kundu, B., Paul, G. C., Mukherjee, K., Pradhan, B., Dikshit, A., Maulud, K. N. A., & Alamri, A. M. (2021). Spatial assessment of drought vulnerability using fuzzy-analytical hierarchical process: a case study at the Indian state of Odisha. *Geomatics, Natural Hazards and Risk*, 12(1), 123-153.
- Saini, S. S., Jangra, R., & Kaushik, S. P. (2015). Vulnerability assessment of soil erosion using geospatial techniques-A pilot study of upper catchment of Markanda river. *International journal of advancement in remote sensing, gis and geography*, 2(1), 9-21.
- Schoennagel, T., Veblen, T.T., & Romme, W.H. (2004). The interaction of fire, fuels, and climate across rocky mountain forests. *Bioscience* 54(7), 661–676
- SDMP. (2017). State Disaster Management Plan. India: Department of Disaster Management, Relief, Rehabilitation and Construction, Government of Jammu and Kashmir
- Seejata, K., Yodying, A., Wongthadam, T., Mahavik, N., & Tantanee, S. (2018). Assessment of flood hazard areas using analytical hierarchy process over the Lower Yom Basin, Sukhothai Province. *Procedia engineering*, 212, 340-347.
- Shah, A., Qadri, T., & Khwaja, S. (2018). Living with earthquake hazards in South and Southeast Asia. *ASEAN J. Commun. Engage*, 2, 15–37.

- Sharma, S. (2019). Impact of Anthropogenic Activities on the Sustainability of Wetlands in Jammu Province. Thesis submitted to University of Jammu. Retrieved from <http://hdl.handle.net/10603/325420>
- Sharma, S., Kumar, A., & Ghangas, V. (2013). Seismicity in Jammu and Kashmir region with special reference to Kishtwar. *International Journal of Scientific and Research Publications*, 3(9), 1-5.
- Shekhar, S., & Pandey, A. C. (2015). Delineation of groundwater potential zone in hard rock terrain of India using remote sensing, geographical information system (GIS) and analytic hierarchy process (AHP) techniques. *Geocarto Int.*, 30(4), 402–421
- Singh, V., Yadav, R. R., Gupta, A. K., Kotlia, B. S., Singh, J., Yadava, A. K., ... & Misra, K. G. (2017). Tree ring drought records from Kishtwar, Jammu and Kashmir, northwest Himalaya, India. *Quaternary International*, 444, 53-64.
- Swain, K. C., Singha, C., & Nayak, L. (2020). Flood susceptibility mapping through the GIS-AHP technique using the cloud. *ISPRS International Journal of Geo-Information*, 9(12), 720.
- Thayyen, R., Dimri, A., Kumar, P., & Agnihotri, G. (2013). Study of cloudburst and flash floods around Leh, India, during August 4–6, 2010. *Natural hazards*, 65, 2175– 2204. doi: 10.1007/s11069-012-0464-2
- Theilen-Willige, B. (2010). Detection of local site conditions influencing earthquake shaking and secondary effects in Southwest-Haiti using remote sensing and GIS methods. *Nat Hazards Earth Syst Sci.*, 10(6), 1183–1196.
- Tilloy, A., Malamud, B. D., Winter, H., & Joly-Laugel, A. (2019). A review of quantification methodologies for multi-hazard interrelationships. *Earth-Science Reviews*, 196, 102881.
- Ullah, K., & Zhang, J. (2020). GIS-based flood hazard mapping using relative frequency ratio method: A case study of Panjkora River Basin, eastern Hindu Kush, Pakistan. *PLoS One* 15, e0229153.
- Ullah, K., Wang, Y., Fang, Z., Wang, L., & Rahman, M. (2022). Multihazard susceptibility mapping based on Convolutional Neural Networks. *Geoscience Frontiers*, 13, 101425. <https://doi.org/10.1016/j.gsf.2022.101425>
- United Nations Office for Disaster Risk Reduction (UNDRR). (2022). Global Assessment Report on Disaster Risk Reduction 2022: Our World at Risk: Transforming Governance for a Resilient Future. Geneva.
- Van Westen, C. (2011). Remote sensing and GIS for Natural Hazard Assessment and Disaster Risk Management. Retrieved from www.cdema.org/virtualimages/background/
- van Westen, C. J., & Greiving, S. (2017). Multi-hazard risk assessment and decision making. In N. R. Dalezios (Ed.), *Environmental hazards Methodologies for Risk Assessment and Management* (pp. 31-94). IWA Publishing
- Yalcin, A. (2008). GIS-based landslide susceptibility mapping using analytical hierarchy process and bivariate statistics in Ardesen (Turkey): comparisons of results and confirmations. *CATENA*, 72(1), 1-12.
- Yalcin, G., & Akyurek, Z. (2004). Analysing flood vulnerable areas with multicriteria evaluation. In *20th ISPRS congress* (pp. 359-364).

- Ying, X., Zeng, G.M., Chen, G. Q., Tang. L., Wang, K.L., & Huang, D.Y. (2007). Combining AHP with GIS in synthetic evaluation of eco-environment quality—a case study of Hunan Province, China. *Ecol Model*, 209(24), 97–109
- Yousuf, M., & Dar, A., & Bukhari, K. (2017). Landslide hazard and risk analysis of national highway-1a (NH-1a) from Jammu to Anantnag: implications to landslide risk reduction.
- Zizovic, M., Marinkovik, D., & Boza, M. (2020). Objective methods for determining criteria weight coefficients: a modification of the CRITIC method. *Decision Making: Applications in Management and Engineering*, 3, 149–161. doi: 10.31181/dmame2003149z